Running Title: Immunoglobulin M regulates airway hyperresponsiveness independent of T helper 2 allergic inflammation.

Authors and Affiliations:

Sabelo Hadebe[a*], Anca Flavia Savulescu[b], Jermaine Khumalo[a], Katelyn Jones[a], Sandisiwe Mangali[a,c], Nontobeko Mthembu[a], Fungai Musaigwa[a], Welcome Maepa[b], Hlumani Ndlovu[b], Amkele Ngomti[a,] Martyna Scibiorek[a,c], Javan Okendo[b,e], Frank Brombacher[a,c,d*]

[a]Division of Immunology, Department of Pathology, Faculty of Health Sciences, University of Cape Town, Cape Town, South Africa

[b]Division of Chemical, Systems & Synthetic Biology, Faculty of Health Sciences, Institute of Infectious Disease & Molecular Medicine, University of Cape Town, Cape Town, South Africa

[c]International Centre for Genetic Engineering and Biotechnology (ICGEB) and Institute of Infectious Diseases and Molecular Medicine (IDM), Division of Immunology, Health Science Faculty, University of Cape Town, Cape Town, South Africa

[d]Wellcome Centre for Infectious Diseases Research in Africa (CIDRI-Africa), Institute of Infectious Diseases and Molecular Medicine (IDM), Faculty of Health Sciences, University of Cape Town, Cape Town, 7925, South Africa

[e]Centre for Research in Therapeutic Sciences (CREATES), Strathmore University, Nairobi, Kenya

26 * **Corresponding Author**: Professor Frank Brombacher

27 International Centre for Genetic Engineering and Biotechnology (ICGEB) and Institute

28 of

29 Infectious Diseases and Molecular Medicine (IDM), Division of Immunology, Health

30 Science

31 Faculty, University of Cape Town, Cape Town, South Africa

32 Email: brombacherfrank@gmail.com

33 Tel: +27 21 406 6424

34 Fax: +27 21 406 6938

35

36 * **Corresponding author:** Dr Sabelo Hadebe

37 Division of Immunology, Health Science Faculty, University of Cape Town, Cape

38 Town, South Africa

39 Email: sabelo.hadebe@uct.ac.za

40 Tel: +27 21 406 6161

41 Fax: + 27 21 406 6029

42

43

Abstract

Allergic asthma is a disease driven by T helper 2 (Th2) cells, eosinophilia, airway hyperresponsiveness (AHR) and IgE-secreting B cells. Asthma is largely controlled by corticosteroids and β_2 adregenic receptor agonists that target and relax airway smooth muscle (ASM). Immunoglobulin M (IgM) isotype secreted by naïve B cells is important for class switching but may have other undefined functions.

We investigated the role of IgM in a house dust mite (HDM)-induced Th2 allergic asthma model.

We sensitised wild-type (WT) and IgM-deficient ($IgM^{-/-}$) mice with HDM and measured AHR, and Th2 responses. We performed RNA sequencing on the whole lung of WT and $IgM^{-/-}$ mice sensitised to saline or HDM. We validated our AHR data on human ASM by deleting genes using CRISPR and measuring contraction by single-cell force cytometry.

We found IgM to be essential in AHR but not Th2 airway inflammation or eosinophilia. RNA sequencing of lung tissue suggested that IgM regulated AHR through modulating brain-specific angiogenesis inhibitor 1-associated protein 2-like protein 1 (*Baiap2l1*) and other genes. Deletion of *BAIAP2L1* led to a differential reduction in human ASM contraction when stimulated with TNF-α and Acetylcholine, but not IL-13.

These findings have implications for future treatment of asthma beyond current therapies.

Keywords: Immunoglobulin M, B cells, airway hyperresponsiveness, airway smooth muscle; TH2 cells; single cell force cytometry; fluorescently labelled elastomeric contractible surface; CRISPR-Cas9; *BAIAP2L1*

69 **INTRODUCTION**

70 Immunoglobulin M (IgM) is the first antibody isotype expressed during B cell
71 development and the first humoral antibody responder, conserved across all species
72 from zebrafish to humans [1]. IgM can be divided into natural and antigen-induced IgM
73 and can either be membrane-bound IgM-type B cell receptor (BCR) or secreted IgM
74 [2,3]. Natural IgM plays multiple roles in homeostasis including scavenging and
75 clearance of apoptotic cell debris in conjunction with phagocytic macrophages, B cell
76 survival through tonic signals, lymphoid tissue architecture and prevention of
77 autoimmune diseases [4–6]. At mucosal sites, both natural and antigen-induced IgM play
78 a role in shaping healthy microbiota and IgM repertoire is also shaped by microbiota
79 [7,8]. Secreted IgM antigen complexes can connect signals via unique and shared
80 receptors, suggestive of a more pleiotropic role in homeostasis and disease states [9–
81 11].

82 Natural IgM and secreted IgM are essential in many infectious and non-infectious
83 diseases including those induced by parasites, fungi, bacterial, viral and autoimmune
84 diseases [11]. In *Plasmodium falciparum*, anti-α-gal IgM and anti-MSP1 directed
85 antibodies are protective against primary and secondary infections [12,13]. Mice deficient
86 of secreted IgM are susceptible to pulmonary *Cryptococcus neoformans* and *P. carinii*
87 infection partly due to reduced activation of innate and adaptive responses [14,15]. At
88 mucosal surfaces, IgM promotes healthy gut bacteria that is beneficial for homeostasis
89 such as Firmicutes and Bacteroidetes [16]. Natural and induced secreted IgM produced
90 mainly by B1a cells is protective against *Streptococcus pneumoniae* and *Francisella*
91 *tularensis* infection [17,18]. In these settings, the protective effects of sIgM depended on

92 cytokines IL-1β and GM-CSF [17,18]. The involvement of natural or induced IgM in allergic
93 asthma is unknown, despite selective IgM syndrome dominated by asthma patients [19].
94
95 Asthma is a T helper 2 (Th2) disease characterised by eosinophilic lung inflammation,
96 mucus production, airway hyperresponsiveness (AHR), Th2 cytokines (interleukin-4
97 (IL-4), IL-5 and IL-13) and B cells producing IgE [20]. IgM is central to class switch
98 recombination that results in IgE class-switched B cells [21]. We and others recently
99 showed that the role of B cells in asthma is complex, where the load of the antigen is
100 crucial in their function [22–24]. Mice deficient of B cells ($\mu MT^{-/-}$) can mount exaggerated
101 AHR when challenged with house dust mite (HDM) [24–26] or ovalbumin (OVA) [27–29] partly
102 due to lack of regulatory B cells that dampen AHR [23]. Furthermore, interleukin 4
103 receptor alpha signalling in B cells is required for optimal Th2 allergic airway
104 inflammation through regulation of AHR, germinal centre (GC) formation and B
105 effector 2 function [22].
106
107 Interestingly, B cell isotypes show unique functions in allergic asthma, for example,
108 IgE and its high-affinity receptor, FcεR are redundant in an HDM model [30], whereas
109 IgD plays an amplifying and regulatory role in various allergic models [31]. In this context,
110 IgD activates basophils to secrete IL-4 and Th2 induction during the sensitisation stage
111 through binding basophils via galectin-9 and CD44. Once Th2 responses have been
112 amplified, IgD ligation blocked IgE-mediated basophil degranulation through
113 competing for antigen and inhibiting FcεR mediated signalling [31]. How IgM isotype
114 contributes in the development of allergic asthma is unclear. It is also unclear whether
115 secreted IgM plays different roles compared to membrane-bound IgM, which is more
116 likely to undergo class switching to IgE. We challenged mice lacking both membrane

and secreted IgM with HDM and other allergens and found a profound reduction in AHR. RNA sequencing of lung tissue showed a downregulation of brain-specific angiogenesis inhibitor 1-associated protein 2-like protein 1 (*Baiap2l1*) and erythroid differentiation regulatory factor 1 (*Erdr1*) genes associated with actin cytoskeleton and rearrangement smooth muscle contraction. As a proof of principle, we showed in human smooth muscle cell line that deletion of these genes via CRISPR- resulted in a reduction in smooth muscle contraction at a single cell level. These are unexpected functions of secreted, and membrane-bound IgM; namely, its involvement in modulating airway smooth muscle contraction.

128 **METHODS**

129 **Mice**

130 IgM-deficient homozygotes mice on Balb/C background and on C57BL/6 background
131 were backcrossed at least 10 generations [32]. Wild type on Balb/C and C57BL/6
132 backgrounds were used as a littermate control. Mice were housed in independently
133 ventilated cages under specific pathogen-free conditions at the University of Cape
134 Town Animal Facility. All mice were used at eight to 10 weeks of age and animal
135 procedures were performed according to the strict recommendation by the South
136 African Veterinary Council and were approved by the University of Cape Town Animal
137 Ethics Committee (Reference number 014/019, 018/013 and 022/014).

138

139 **House Dust-mite induced allergic airway disease**

140 A high dose and a low dose HDM treatment schedule were used to induce symptoms
141 of allergic asthma in mice [22]. Mice were anaesthetised with ketamine (Anaket-V;
142 Centaur Labs, Johannesburg, South Africa) and xylazine (Rompun; Bayer, Isando,
143 South Africa). For low-dose HDM, mice were sensitised intratracheally (i.t.) on day 0
144 with 1 µg of HDM (Stellergens Greer Laboratories, Lenoir, U.S.A.) and intranasally
145 challenged with 3 ug HDM on days 8, 9, 10, 11 and 12. For high-dose HDM, mice
146 were with HDM 100 ug and challenged with HDM 10 ug. AHR was measured on day
147 15. After the procedure, mice were euthanised and tissue samples were collected for
148 analysis.

149

150 **Adoptive transfer of naïve B cells**

151 Spleens were collected from naïve congenic CD45.1 Balb/C mice and passed through
152 40µm strainer to obtain single-cell suspensions. Cells were stained with FITC-B220

153 and APC-CD19 for 30min at 4°C. A dead cell exclusion dye (7AAD) was added before
154 sorting on BD FACS Aria I to at least 96% purity. 2-5 x 10^6 cells were adoptively
155 transferred intravenously (i.v.) into $IgM^{-/-}$ recipient mice a day before HDM
156 sensitisation.
157
158 **Adoptive transfer of naïve serum**
159 Naïve wild-type mice were euthanised and blood was collected via cardiac puncture
160 before being spun down (5500rpm, 10min, RT) to collect serum. Serum (200μL) was
161 injected intraperitoneally into IgM-deficient mice. Serum was injected intraperitoneally
162 at day -1, 0, and a day before the challenge with HDM (day 10).
163
164 **Busulfan Bone marrow chimeras**
165 WT (CD45.2) and $IgM^{-/-}$ (CD45.2) congenic mice were treated with 25 mg/kg busulfan
166 (Sigma-Aldrich, Aston Manor, South Africa) per day for 3 consecutive days (75 mg/kg
167 in total) dissolved in 10% DMSO and Phosphate buffered saline (0.2mL,
168 intraperitoneally) to ablate bone marrow cells. Twenty-four hours after last
169 administration of busulfan, mice were injected intravenously with fresh bone marrow
170 (10x10^6 cells, 100μL) isolated from hind leg femurs of either WT (CD45.1) or $IgM^{-/-}$
171 mice [33]. Animals were then allowed to complement their haematopoietic cells for 8
172 weeks. In some experiments the level of bone marrow ablation was assessed 4 days
173 post-busulfan treatment in mice that did not receive donor cells. At the end of
174 experiment level of complemented cells were also assessed in WT and $IgM^{-/-}$ mice
175 that received WT (CD45.1) bone marrow.
176
177

178 **Ovalbumin-induced allergic airway inflammation**

179 Mice were sensitised intraperitoneally with (50µg in 200µl) of ovalbumin (OVA)
180 adsorbed to 0.65% alum (Sigma-Aldrich, Aston Manor, South Africa) on days 0, 7, 14.
181 On days 23, 24, 25, mice were intranasally challenged with 100µg of OVA under
182 anaesthesia with ketamine (Anaket-V; Centaur Labs, Johannesburg, South Africa)
183 and xylazine (Rompun; Bayer, Isando, South Africa). AHR was measured on day 26.
184 After the procedure, mice were euthanized with halothane and tissue samples
185 collected for analysis.

186

187 **Papain-induced lung inflammation**

188 Mice were anaesthetized with isoflourane (3L/min) briefly before being challenged with
189 50µL of 25 µg of Papain (Sigma-Aldrich, Aston Manor, South Africa) on days 1, 2 and
190 3 or PBS. AHR was measured on day 4. After the procedure, mice were euthanized
191 with halothane and tissue samples collected for analysis.

192

193 **Airway Hyperresponsiveness**

194 Airway resistance and elastance of the whole respiratory system (airways, lung chest
195 wall) after intranasal challenge was determined by forced oscillation measurements
196 as described previously [34] with the Flexivent system (SCIREQ, Montreal, Canada) by
197 using the single compartment (''snapshot'') perturbation. Measurements were carried
198 out with increasing doses of acetyl-β-methylcholine (methacholine, Sigma-Aldrich,
199 Aston Manor, South Africa) (0, 5, 10, 20 and 40 mg/mL) for Balb/C or (0, 20, 40, 80
200 160 and 320 mg/mL) for C57BL/6. Differences in the dose-response curves were
201 analysed by repeated-measures Two-way ANOVA with the Bonferroni post-test. Only

202 mice with acceptable measurements for all doses (coefficient of determination >0.90)
203 were included in the analysis.
204
205 **Flow cytometry**
206 Single-cell suspensions were prepared from lymph nodes in Roswell Park Memorial
207 Institute (RPMI) media (Gibco, Paisley, United Kingdom) by passing them through
208 100µm strainer. To obtain single cell suspensions from lung tissues, a left lobe was
209 digested for 1 hour at 37°C in RPMI containing 13 mg/mL DNase I (Roche, Randburg,
210 South Africa) and 50 U/mL collagenase IV (Gibco, Waltham, Massachusetts) and
211 passed through 70µm strainer. Antibodies used in these experiments included,
212 phycoerythrobilin (PE)- conjugated anti-Siglec-F (clone, E50-2440), anti-IL-5 (clone,
213 TRFK5), anti-CD44 (clone, KM114), anti- T and B cell activation antigen (clone, GL7),
214 anti-CD43 (clone, S7), FITC- conjugated anti-Ly6G (clone, 1A8), anti-IgD (clone, 11-
215 26C2a), IL-4 (clone, 11B11), anti-PD-1-(clone, 29F.1A12), PerCP Cy5.5- conjugated
216 anti-Ly6C (clone, AL-21), -CD45.1 (clone, A20), anti-IL-17 (clone, TC11-18H10), anti-
217 mouse alpha muscle actin (Abcam, ab8211-500), Allophycocyanin (APC)- conjugated
218 anti-CD11c (clone, HL3), anti-CD5 (clone, 53-7.3), BV421 conjugated anti-CD11b
219 (clone, M1/70), anti-CD62L (clone, MEL-14), anti-IgG1 (clone, A110-1), AlexaFlour
220 700- conjugated anti-CD3ε (clone, 145-2C11) -anti-IFN-γ (clone, XMG1.2), BV510-
221 anti-CD4 (clone, RM4-5) and anti- B220 (clone, RA3-6B2), APC-Cy7-conjugated anti-
222 CD19 (clone, 1D3) and anti-CD8 (clone, 53-6.7), BV786 conjugated anti-IgE (clone,
223 R35-72) and anti-IL-33R (ST2) (clone, U29-93), biotin-conjugated anti-IgM (clone, AF-
224 78), anti-CD95 (clone, Jo2), anti- CD249 (clone, BP-1) , anti-CD45 (clone, 30-F11)
225 were purchased from BD Pharmingen (San Diego, CA). PE-Cynanine7 anti-F4/80
226 (clone, BM8), anti-IL-13 (clone, eBio13A), anti-CXCR5 (clone, L138D7), AlexaFlouro

227 700- conjugated anti-MHC II (clone, M5/114), Rabbit anti-BAIAP2L1 (Abcam,
228 PA554000), Live/dead Fixable Yellow stain (Qdot605 dead cell exclusion dye) were
229 purchased from eBiosciences. Biotin-labelled antibodies were detected by Texas Red
230 conjugated PE (BD Biosciences). PE-Goat anti-Rabbit IgG (Abcam, ab72465) was
231 used to detect Rabbit anti-BAIAP2L1. For staining, cells (1 x 10^6) were stained and
232 washed in PBS, 3% FCS FACS buffer. For intracellular cytokine staining, cells were
233 restimulated with phorbal myristate acetate (Sigma-Aldrich) (50 ng/mL), ionomycin
234 (Sigma-Aldrich) (250ng/mL), and monensin (Sigma-Aldrich) (200mM in IMDM/10%
235 FCS) for 5h at 37˚C then fixed in 2% PFA, permeabilised with Foxp3 transcriptional
236 factor staining buffer kit (eBioscience) before intracellular staining with appropriate
237 cytokine antibodies and acquisition through LSR Fortessa machine (BD
238 Immunocytometry system, San Jose, CA, USA) and data was analysed using Flowjo
239 software (Treestar, Ashland, OR, USA).
240
241
242 **Histology**
243 Left upper lung lobes was fixed in 4% formaldehyde/PBS and embedded in paraffin.
244 Tissue sections were stained with periodic acid-Schiff for mucus secretion, and
245 haematoxylin and eosin (H&E) stain for inflammation. Slides were scanned at 20x
246 magnification on the virtual slide VS120 microscope (Olympus, Japan). Downstream
247 processing of images was done through Image J (FIJI) for image extraction at series
248 15 and Ilastik software was used for mucus area quantification on whole lung sections.
249 The data shown are representative of 1 experiment of 3 independent experiments (n
250 = 5-7 mice per experiment).
251

252 **Antibody and cytokine ELISAs**

253 Antibody ELISAs were carried out as previously described[34] using 10 μg/ml HDM to
254 coat for specific IgGs. Total IgE in serum was measured using anti-mouse IgE (BD
255 Biosciences, 553413) to coat, mouse IgE (κ, anti-TNP, BD Biosciences, 557079) as
256 standard and biotin anti-mouse IgE (BD Biosciences, 553419) as a secondary
257 antibody.

258 For *in vitro* cytokine production analysis, single-cell suspensions were prepared from
259 mediastinal lymph nodes of HDM-treated and littermate control mice. Cells ($2x10^5$
260 cells, in 200μL) were incubated for 5 days in RPMI/10% FCS (Delta Bioproducts,
261 Kempton Park, South Africa) in 96-well plates. Cells were either stimulated with HDM
262 (30μg/mL) or plate bound anti-CD3 (10μg/mL) and supernatants were collected after
263 a 5-day incubation period. Concentrations of IL-4, IL-5 (BD Biosciences) and IL-13
264 (R&D Systems, Minneapolis, Minn), were measured using ELISA assays according to
265 the manufacturer's protocol.

266

267 **RNA Extraction**

268 Small lung lobe was frozen in Qiazol (Qiagen, Germany) and stored at −80°C. Total
269 RNA was isolated from the lysate using miRNeasy Mini kit (Qiagen, Germany)
270 according to the manufacturer's instructions. RNA quantity and purity were measured
271 using the ND-1000 NanoDrop spectrophotometer (ThermoScientific, DE, USA).

272

273 **cDNA Synthesis and RT-qPCR**

274 For *Muc5a* gene expression analysis, 100 ng total RNA was reverse transcribed into
275 cDNA using Transcriptor First Strand cDNA Synthesis Kit (Roche, Germany)
276 according to the manufacturer's instructions. Quantitative real-time PCR (RT-qPCR)

277 was performed using LightCycler® 480 SYBR Green I Master (Roche, Germany) and
278 *Muc5a* primers (IDT, CA, USA). Fold change in gene expression was calculated by
279 the ΔΔCt method and normalized to ß-*actin* which was used as an internal control.
280

281 **Whole lung RNA sequencing**

282 Whole lung RNA was extracted using RNAeasy kit (Qiagen, Germany) according to
283 the manufacturer's instructions. We used Agilent 2100 Bio analyzer (Agilent RNA 6000
284 Nano Kit) to do the total RNA sample QC: RNA concentration, RIN value,28S/18S and
285 the fragment length distribution. The first step in the workflow involved purifying the
286 poly-A containing mRNA molecules using poly-T oligo attached magnetic beads.
287 Following purification, the mRNA was fragmented into small pieces using divalent
288 cations under elevated temperature. The cleaved RNA fragments were copied into
289 first strand cDNA using reverse transcriptase and random primers. This was followed
290 by second strand cDNA synthesis using DNA Polymerase I and RNase H. These
291 cDNA fragments had addition of a single 'A' base and subsequent ligation of the
292 adapter. The products were then purified and enriched with PCR amplification. PCR
293 yields were quantified by Qubit and pooled samples together to make a single strand
294 DNA circle (ssDNA circle), which gave the final library. DNA nanoballs (DNBs) were
295 generated with the ssDNA circle by rolling circle replication (RCR) to enlarge the
296 fluorescent signals at the sequencing process. The DNBs were loaded into the
297 patterned nanoarrays and pair-end reads of 100 bp were read through on the DNBseq
298 platform for the following data analysis study. For this step, the DNBseq platform
299 combines the DNA nanoball-based nanoarrays and stepwise sequencing using
300 Combinational Probe-Anchor Synthesis Sequencing Method.
301

302 **Bioinformatics workflow**

303 The ribosomal RNA (rRNA) was first removed using SortMeRNA. We then did the
304 Fastq file quality control using Fastqc and multiqc software to assess the quality of the
305 raw reads followed by adapter trimming using Trim galore. The reads were then
306 aligned to the mouse reference genome (mm10_UCSC_20180903) using STAR
307 aligner. The map read counts was then extracted using featurecounts. The gene
308 differential analysis was conducted using the DEseq2. The genes with LFC >= 2 and
309 adjusted p-value <= 0.05 was used to do the gene ontology over-representation
310 analysis done using clusterProfiler[35] Bioconductor package. The Benjamini-Hochberg
311 method was used for multiple test correction.

312

313 **Human bronchial Airway Smooth Muscle cell culture**

314 A healthy human bronchial smooth muscle cell line (BSMC, Lonza) was cultured in
315 Smooth Muscle Growth Medium (Lonza) supplemented with Insulin (CC-4021D),
316 human Fibroblastic Growth Factor-B (CC-4068D), Gentamicin sulfate-Amphotericin-
317 1000 (CC-4081D), 5% Foetal Bovine Serum (CC-4102D), human Epidermal Growth
318 Factor (CC-4230D) (all purchased from Lonza) in a T25 flask (Lonza) until confluence.
319 After two passages in the T75 flask, confluent cells were seeded at 1.6×10^5 BSMC
320 cells onto 24-well trays and immediately transfected with CRISPR/Cas9 single guide
321 RNAs.

322

323 **CRISPR/Cas9 single guide RNA transfections**

324 single guide RNAs targeting human *BAIAP2L1* (# CD.Cas9.CXVQ6494.AA); *ERDR1*,
325 (# CD.Cas9.YFVV2490.AA); HPRT Negative Control (#Alt-R® CRISPR-Cas9crRNA)
326 were purchased (IDT, CA, USA via WhiteScientific PTY LTD). Single guide RNA (1

327 μM) and Cas9 enzyme (1 μM) in Opti-MEM medium (Life Technologies™, Carlsbad,
328 CA, USA) were transfected using Lipofectamine RNAi Max 1000 (Thermo Scientific)
329 into BSMC cells (1.6 x10^5) per well and either stimulated with Acetylcholine (10μM),
330 recombinant human IL-13 (100 ng/mL), recombinant human TNF-α (10 ng/mL) or left
331 unstimulated for 48 hours at 37°C, 5% CO_2 incubator. Gene deletion was confirmed
332 by DNA extraction (Wizard Genomic DNA Purif. Kit, Promega) and PCR amplification
333 of target genes using *BAIAP2L1* forward (GTCCCGGGGGCCCGA) and reverse
334 (AAGCGCCCAAGAATGTGGGG) primers, and product run on a 1.2% agarose gel.
335

336 **Cytotoxic detection Assay**

337 To measure cytotoxicity after single guide RNA transfection, lactate dehydrogenase
338 (LDH) was measured in supernatants collected at 48 hours post transfection using
339 cytotoxicity detection kit ^{PLUS} Assay (CYTODET-RO, Roche) according to
340 manufacturer's instructions and plates were read at 490 nm.
341

342 **Single-cell force cytometry using Fluorescently Labelled Elastomeric**
343 **Contractible Surface (FLECS) technology**

344 BSMCs were seeded on Fibronectin-coated elastomeric micropatterns (Forcyte
345 Biotechnologies #F2AX0G03Y, 50 microns, Alexa Fluor 488 - bound Fibrinogen, 24-
346 well plate) at a concentration of 75,000 cells per well in Smooth muscle growth medium
347 (SmGM) (Lonza) and left to adhere and spread for 90 minutes. Unattached cells were
348 then removed and fresh SmGM medium supplemented with rhTNF-α (10 ng/mL)/rhIL-
349 13 (100 ng/mL)/ACh (10μM) was added. BSMCs were stimulated for 3 hrs before
350 being fixed in pre-warmed to 37°C 4% PFA. Fixed samples were washed and then
351 stained with ATTO-565 phalloidin (ATTO-TEC) and DAPI (Life Technologies) and

352 imaged on a StellarVision microscope using Synthetic Aperture Optics technology
353 (Optical Biosystems). All images were analyzed using FiJi software by measuring the
354 length of each micropattern per condition after stimulation and subtracting the length
355 of the unstimulated micropattern of the same condition.
356
357 **Immunofluorescent**
358 Left upper lung lobes were fixed in 4% formaldehyde/PBS and embedded in paraffin.
359 Tissue sections (5 μm) were deparaffinised and hydrated in water before antigen
360 retrieval in boiling 10 mM Citrate buffer (pH 6, pressure cooker for 2 mins). Tissue was
361 incubated with Rabbit anti-BAIAP2L1 (Abcam, PA554000) in PBS-Tween (1:250,
362 overnight, 4°C) and FITC anti-mouse alpha muscle actin (Abcam, ab8211-500, 1:100,
363 overnight, 4°C). Tissues were washed with PBS-Tween before incubation with
364 secondary antibody PE-Goat anti-Rabbit IgG (Abcam, ab72465) in PBS-Tween
365 (1:500, RT in the dark for 30min). Tissues were washed with PBS-Tween before
366 mounting in DAPI mounting media (Thermofisher). Fluorescent images were captured
367 at 60x magnification using LSM880 Airy Scan (Zeiss, UK).
368
369 **Western blotting**
370 Protein harvest: RIPA lysis buffer supplemented with protease inhibitors was added to
371 the lung tissue. The whole-cell lysates were incubated on ice for 20 min and vortexed
372 every 5 min for 60 seconds. Then, the lysate was centrifuged at 3000 rpm for 15
373 minutes at 4°C, and the supernatant was collected. Total protein concentrations were
374 determined using the Pierce BCA Assay kit.
375

376 SDS-PAGE: 20 µg of each protein sample was mixed with Laemmli buffer and heated
377 for 10 minutes at 100 °C. Equal amounts of protein samples were loaded into 5%
378 acrylamide stacking gel and a 12% acrylamide separating gel along with 5 µL
379 PageRulerTM Plus Prestained protein ladder (catalogue #: 26619, Thermo
380 ScientificTM) and separated by electrophoresis at 100 V. Proteins were transferred
381 onto nitrocellulose membranes (Bio-Rad) using the Bio-Rad Mini Trans-Blot® Cell
382 according to the manufacturer's instructions.
383
384 After protein transfer, the nitrocellulose membranes were stained with Ponceau stain
385 for approximately 1-3 minutes to visualize if the proteins had been transferred. Once
386 the protein bands were identified, the membrane was washed with ddH_2O until 80%
387 of the Ponceau staining is removed. The remaining 20% of the stain allowed the
388 accurate segmentation of the membrane to separate high molecular weight proteins
389 from low molecular weight proteins. The nitrocellulose membranes were blocked with
390 5 % (w/v) non-fat milk, 0.01% Tween-20 in TBST) on the shaker at room temperature
391 for one hour. The low and high molecular weight membranes proteins were incubated
392 with respective primary antibodies (Rabbit anti-human BAIAP2L1, PA5-54000,
393 Invitrogen) or (Goat anti-mouse GAPDH, sc 365062, Santa Cruz) overnight shaking
394 in the 4°C cold room. Membranes were washed 4 times with 1xTBST in 15-minute
395 intervals. Horseradish peroxidase (HRP) secondary antibodies were added to their
396 respective membranes and incubated for one hour at room temperature, with shaking.
397 subsequently, membranes were washed 3 times in 1xTBST in 15 minutes intervals.
398 To visualise the protein bands on autoradiographic film (Santa Cruz Biotechnology®),
399 Lumino Glo® substrate kit was added to each membrane. Briefly, the substrate luminol

400 was oxidised by hydrogen peroxide in the presence of the catalyst HRP to yield a
401 chemiluminescent product.
402
403 **Plating of faecal pellets to confirm a reduction in bacterial colonies following**
404 **antibiotic treatment.**
405 The faecal pellet was collected from each individual mouse treated with antibiotics as
406 well as control groups not treated with antibiotics. The faecal pellet was weighed and
407 resuspended in sterile PBS at a concentration of 50 mg/mL. The sample was
408 resuspended until homogenous, and 1/100 dilution was made in sterile PBS. 50μL of
409 1/100 dilutions was plated on tryptic soy agar plates and spread evenly across the
410 plate before incubating at 37°C for 16 hrs. Individual colonies were counted manually.
411
412 **Statistical analysis**
413 P-values were calculated in GraphPad Prism 6 (GraphPad Software, Inc) by using
414 nonparametric Mann-Whitney Student's t-test or Two-way ANOVA with Bonferroni's
415 post-test for multiple comparisons, and results are presented as standard error of the
416 mean (SEM) or mean of standard deviation (SD). Differences were considered
417 significant if P was <0.05.
418
419

420 **RESULTS**

421 **IgM-deficient mice show profound airway hyperresponsiveness reduction when**
422 **exposed to HDM.**

423 We sensitised and challenged IgM-deficient (IgM$^{-/-}$) and wild-type Balb/c (WT) mice
424 with HDM intratracheally (i.t.) and analysed AHR, lung infiltrates and cytokines (Fig.
425 1a, Supplementary Fig. 1a). We found moderately reduced resistance and elastance
426 in IgM$^{-/-}$ sensitised with a high dose of HDM (100μg) compared to WT mice
427 (Supplementary Fig. 1b). Similarly, we also observed a profound reduction in AHR in
428 IgM$^{-/-}$ mice sensitised with a low dose of HDM (1μg) compared to WT (Fig. 1b).
429 Interestingly, lung eosinophils were intact at both low dose (Fig. 1c) and high dose
430 HDM (Supplementary Fig. 1d). We could also show that AHR reduction in IgM$^{-/-}$ mice
431 was not allergen-specific, as we observed similar findings using ovalbumin (OVA)
432 complexed to alum adjuvant (Supplementary Fig. 2a-b) and acute papain-induced
433 allergic inflammation (Supplementary Fig. 2c-d). We observed similar finding of
434 profound AHR reduction in IgM$^{-/-}$ mice in C57BL/6 background compared to WT mice
435 (Supplementary Fig. 3a). These findings suggested that IgM-deficient mice have
436 profound AHR reduction independent of allergen or mice background strain.

437

438 **IgM deficiency does not impact B cell subsets in primary and secondary organs,**
439 **but class switching is impaired.**

440 We also observed no significant changes between IgM$^{-/-}$ and WT mice in mucus
441 production shown by *Muc5a* gene expression (Fig. 1d) or goblet cells in Balb/C
442 (Supplementary Fig. 1f) and C57BL/6 mice challenged with HDM (Supplementary Fig.
443 3b). Accompanying reduction in AHR in IgM$^{-/-}$ mice was low titers of total IgE, HDM-
444 specific IgE, and mediastinal lymph node (mLN) B cell surface expression of IgM and

445 IgG1 (Fig. 1e-f), owing to a lack of class switching. Interestingly, the numbers of lung
446 B cells were normal (Fig. 1c and Supplementary Fig. 1c) and the frequencies of B cell
447 subsets such as follicular, marginal zones and germinal centres (GCs) B cells were
448 not affected by lack of IgM (Fig. 1g and Supplementary Fig. 1g). The lack in class
449 switching in Balb/C mice was also consistent with what we found in $IgM^{-/-}$ mice in the
450 C57BL/6 background (Supplementary Fig. 3c). This suggested a normal interaction
451 between B and T cells in GCs, but lack of AID-dependent class switching, despite
452 increased expression of IgD (Supplementary Fig. 4a) [36]. We checked for natural IgM
453 and antigen-induced IgM in multiple tissues. B cells expressing IgD were increased in
454 all tissues including mLNs, peritoneal cavity and spleen (Supplementary Fig. 4a-c) and
455 pre-B cell subsets were normal in BM (Supplementary Fig. 4d) in the absence of IgM
456 as previously reported [32].
457

458 **T helper 2 cells are intact in the absence of IgM, and serum transfer can partially**
459 **restore antibody function**

460 To investigate whether the reduction in AHR was due to reduced Th2 cells and
461 cytokines, we stimulated total mLN and lung cells with anti-CD3 for 5 days or with
462 PMA/ionomycin for 5 hrs in the presence of monensin and measured secreted or
463 intracellular IL-4 and IL-13 expression. We found no differences in CD4 T cells and T
464 follicular helper cells (Fig. 2a) in mLN and in secreted or intracellular levels of IL-4 and
465 IL-13 between $IgM^{-/-}$ and WT mice challenged with HDM in both mLN and lungs (Fig.
466 2b-c). To investigate what drives this reduced AHR in the absence of IgM between
467 secreted antibodies or the IgM B cell receptor on the surface of B cells, we transferred
468 serum from naïve WT mice into $IgM^{-/-}$ mice a day before sensitization, during
469 sensitisation and a day before challenge with HDM allergen (Fig. 2d), as previously

470 described [37]. AHR in IgM$^{-/-}$ was still reduced compared to WT mice even after the
471 transfer of WT serum (Fig. 2e), but levels of total IgE, HDM-specific IgE and HDM-
472 specific IgG1 were increased and comparable to those found in WT mice (Fig. 2f and
473 Supplementary Fig. 6d). The redundant role of IgE was consistent with previous
474 studies where IgE nor its high-affinity receptor (FcεRI) were essential in AHR in an
475 HDM or OVA models [30]. The lack of functional role of serum-transferred IgE was
476 consistent with earlier findings on *H. polygyrus* transfer of immune serum where IgE
477 was found not to be essential in protection against *H. polygyrus* re-infection [37].
478
479 **Replacement of IgM-deficient mice with functional hematopoietic cells in**
480 **busulfan mice chimeric mice restores airway hyperresponsiveness.**
481 We then generated bone marrow chimeras by chemical radiation using busulfan [33].
482 We treated mice three times with busulfan for 3 consecutive days and after 24 hrs
483 transferred naïve bone marrow from congenic CD45.1 WT mice or CD45.2 IgM$^{-/-}$ mice
484 (Fig. 3a and Supplementary Fig. 5a). We showed that recipient mice that did not
485 receive donor bone marrow after 4 days post-treatment have significantly reduced
486 lineage markers (CD45^{+}Sca-1^{+}) or lineage negative (Lin-) cells in the bone marrow
487 when compared to untreated or vehicle (10% DMSO) treated mice (Supplementary
488 Figure 5b-c). We allowed mice to reconstitute bone marrow for 8 weeks before
489 sensitisation and challenge with low dose HDM (Figure 3a). We showed that WT
490 (CD45.2) recipient mice that received WT (CD45.1) donor bone marrow had higher
491 airway resistance and elastance and this was comparable to IgM$^{-/-}$ (CD45.2) recipient
492 mice that received donor WT (CD45.1) bone marrow (Figure 3b). As expected, IgM$^{-/-}$
493 (CD45.2) recipient mice that received donor IgM$^{-/-}$ (CD45.2) bone marrow had
494 significantly lower AHR compared to WT (CD45.2) or IgM$^{-/-}$ (CD45.2) recipient mice

495 that received WT (CD45.1) bone marrow (Figure 3b). We confirmed that the
496 differences observed were not due to differences in bone marrow reconstitution as we
497 saw similar frequencies of CD45.1 cells within the lymphocyte populations in the lungs
498 and other tissues (Supplementary Fig. 5d). We observed no significant changes in the
499 lung neutrophils, eosinophils, inflammatory macrophages, CD4 T cells or B cells in
500 WT or IgM$^{-/-}$ (CD45.2) recipient mice that received donor WT (CD45.1/CD45.2) or IgM^{-}
501 $^{/-}$ (CD45.2) bone marrow when sensitised and challenged with low dose HDM (Fig. 3c)
502
503 Restoring IgM function through adoptive reconstitution with congenic CD45.1 bone
504 marrow in non-chemically irradiated recipient mice or sorted B cells into IgM$^{-/-}$ mice
505 (Supplementary Fig. 6a) did not replenish IgM B cells to levels observed in WT mice
506 and as a result did not restore AHR, total IgE and IgM in these mice (Supplementary
507 Fig. 6b-c).
508
509 IgM is known to play key role in shaping gut microbiota and its diversity can be shaped
510 by gut commensals [16,38]. To understand whether microbiota could influence AHR in
511 IgM-deficient mice, we treated WT and IgM$^{-/-}$ with an antibiotic cocktail 3x per week for
512 2 weeks (Supplementary Fig. 7a). We confirmed the reduction of bacteria in the faecal
513 pellet after 2 weeks of antibiotic treatment (Supplementary Fig. 7a). We then
514 sensitised and challenged these mice with HDM and measure AHR (Supplementary
515 Fig. 6b). We observed increased resistance and elastance in WT mice compared to
516 IgM$^{-/-}$ mice and pre-treatment with antibiotics did not influence AHR (Supplementary
517 Fig. 7b). Treatment with antibiotics did increase total IgE, HDM-specific IgE and IgG1
518 in WT mice as expected[39], but had no impact on IgM-deficient mice (Supplementary
519 Fig. 7c), suggesting that overall antibiotics did not influence AHR.

520 **RNA sequencing reveals enrichment of genes associated with skeletal muscle**
521 **contraction and actin re-arrangement.**
522 Because we had found no other changes in asthmatic allergic features between WT
523 and IgM$^{-/-}$, except for profoundly reduced AHR which we could only restore when we
524 partially replaced IgM-deficient haematopoietic cells with WT bone marrow, we
525 resorted to RNA sequencing. We wanted to know if there were lung-specific factors
526 that influenced AHR regulation in IgM-deficient mice. Principal component analysis
527 (PCA) depicted distinct global transcriptional changes with PC1 and PC2 explaining
528 most of the variation (Fig. 4a). We found a smaller variation in gene expression
529 between WT and IgM$^{-/-}$ in both HDM-challenged and PBS control mice (Fig. 4b). We
530 could mainly detect downregulation of genes such as brain-specific angiogenesis
531 inhibitor 1-associated protein 2-like protein 1 (*Baiap2l1*), erythroid differentiation
532 regulatory factor 1 (*Erdr1*), chemokines such as *Ccl8*, *Ccl9*, *Ccl17* and *Ccl22* in IgM$^{-/-}$
533 mice challenged with HDM (Fig. 4c-d). Interestingly, *Baiap2l1* and *Erdr1* were also
534 downregulated in IgM$^{-/-}$ saline-treated control mice, suggesting an inflammation-
535 independent effect (Fig. 4c and e). We also found the presence of the J-chain coding
536 gene in WT mice which was absent in IgM$^{-/-}$ mice, confirming a deletion in genes
537 associated with holding IgM monomers together and thus IgM [40] (Fig. 4e). Gene set
538 enrichment analyses (GSEA) confirmed that the genes contributing to changes in AHR
539 between WT and IgM$^{-/-}$ were associated with muscle system processes and skeletal
540 muscle contraction (Fig. 4f). There was also an over-representation of gene ratios
541 associated with skeletal muscle development, differentiation and contraction, and
542 suppression of genes associated with chemotaxis and plasma membrane-bounded
543 cell projection (Supplementary Fig. 8).
544

545 ***BAIAP2L1* is expressed in lung cells in contact with airway smooth muscle cells.**
546 We decided to focus on *Baiap2l1* also known as Inverse-bin-amphiphysin-Rvs (I-
547 BAR)-domain-containing protein insulin receptor tyrosine kinase substrate (IRTKS),
548 which has been shown to promote actin polymerisation and microvilli length in the
549 intestinal epithelial cells [41]. We first verified whether BAIAP2L1 was also
550 downregulated at the protein level in IgM-deficient mouse lungs challenged with HDM
551 (Fig. 5a). We found lower expression levels of BAIAP2L1 in IgM-deficient mice
552 compared to WT mice challenged with HDM by western blotting, although this was not
553 significant (Fig. 5a). Human Protein Atlas search suggested that BAIAP2L1 is
554 expressed by multiple cell types including fibroblasts, skeletal muscle, smooth muscle
555 and macrophages [42]. We then investigated by immunofluorescence which cell types
556 within the lung could be expressing BAIAP2L1 (Fig. 5b). We found BAIAP2L1 to be
557 closely expressed within structural cells in close contact to smooth muscle cells (less
558 than 10μm), a cell type known to be essential in bronchoconstriction. Airway smooth
559 muscle together with the extracellular matrix contributes to smooth muscle
560 hypertrophy which causes the narrowing of the airways. These cells by histology
561 appear to be separated due to fixation methods but are mashed together, especially
562 during the remodelling of the airways [43]. IgM deficiency did not impact this expression
563 in cells in close contact with smooth muscle (Fig. 5b). Because both western blot and
564 immunofluorescent were inconclusive, we also verified the expression of BAIAP2L1
565 via flow cytometry (gating in Supplementary Fig. 9a) and found it to be expressed
566 mainly by alpha-smooth muscle cells and increased in expression in HDM treated mice
567 compared to PBS control mice (Fig. 5c). Furthermore, we showed a reduction in
568 BAIAP2L1 expression amongst alpha-smooth muscle cells but not other cells (CD45
569 positive or alpha-smooth muscle negative cells, Supplementary Fig. 9b) in IgM-

570 deficient mice compared to WT mice treated with HDM, although this did not reach
571 significance (Fig. 5c). Overall, this data suggested that BAIAP2L1 is reduced at RNA
572 and protein level and likely influenced the reduction of AHR in IgM-deficient mice. This
573 was consistent with gene set enrichment in our RNA seq data where there was a
574 dominance of genes associated with muscle contraction which regulates AHR.
575
576 **CRISPR-Cas9 deletion of *BAIAP2L1* leads to reduced airway smooth muscle**
577 **contraction at a single cell.**
578 To understand how *Baiap2l1*, one of the genes downregulated in IgM-deficient mice,
579 could influence AHR, we resorted to an *in vitro* model that allowed us to measure
580 contraction using fluorescently labelled elastomeric contractible surface (FLECS)
581 technology [44] (Fig. 6a). We opted for airway smooth muscle as it has been shown to
582 contribute to the narrowing of the airway during an allergic attack and together with
583 neighbouring cells such as extracellular matrix and immune cells are critical in
584 hypertrophy [43]. We chose the human bronchial smooth muscle cell (BSMCs) line as
585 *BAIAP2L1* is expressed in structural cells including muscle and epithelial cells, and
586 actin together with myosin is essential in muscle contraction [42]. To this end, we used
587 CRISPR-Cas9 technology to knock down *BAIAP2L1* in BSMCs (Supplementary Fig.
588 10a-b). We also included ERDR1 as one of the genes that were also downregulated
589 in IgM-deficient mice. BSMCs (160 000/well) were stimulated with 10μM acetylcholine
590 (ACh), 10 ng/mL of human TNF-α and 100 ng/mL IL-13, followed by transfection with
591 ribonucleoprotein (RNP) complexes containing single guide RNA targeting *BAIAP2L1*
592 and Cas9 for 48h (Fig. 6b). Transfected cells were seeded onto elastomeric patterns,
593 stimulated with the same stimulants for 3h and fixed in 4% paraformaldehyde, followed
594 by staining with DAPI and Phalloidin before imaging on Stellarvision microscope and

595 quantification (Fig. 6a). We validated the deletion of *BAIAP2L1* by PCR and showed
596 reduced expression of *BAIAP2L1* in ACh and TNF-α stimulated cells transfected with
597 *BAIAP2L1* sgRNA when compared to scramble sgRNA (Supplementary Fig. 10c, line
598 3 and 4 compared to line 5 and 6). We also detected low expression of BAIAP2L1 in
599 unstimulated sgRNA scramble and sgRNA *BAIAP2L1* transfected cells
600 (Supplementary Fig. 10c, lines 1 and 2). Transfections with sgRNA did not impact cell
601 viability (Supplementary Fig. 10d). As expected, BSMCs displayed a higher level of
602 contraction in TNF-α or IL-13 stimulated cells compared to unstimulated cells (Fig. 6b-
603 d). In BSMCs transfected with sgRNA-*BAIAP2L1* and -*ERDR1*, we saw a significant
604 reduction in contraction levels in TNF-α stimulated cells when compared to scramble
605 sgRNA transfected and stimulated cells (Fig. 6b, c). We saw no differences in
606 contraction between scramble sgRNA and sgRNA-*BAIAP2L1* and -*ERDR1* stimulated
607 with IL-13 (Fig. 6d).
608
609 ***BAIAP2L1* deletion but not *ERDR1* is essential in acetylcholine-induced smooth**
610 **muscle contraction.**
611 Contraction of the ASM is central to AHR as it controls airway diameter and airflow
612 which can increase resistance [20]. Airway smooth muscle contractility is induced when
613 extracellular factors such as ACh bind through muscarinic 3 acetylcholine receptor
614 (m_3AChR), activating a signalling cascade leading to calcium accumulation and
615 contraction [45]. We transfected BSMCs with sgRNA-*BAIAP2L1*, -*ERDR1* or scrambled
616 and stimulated cells with 10 μM ACh (Fig. 7a). We saw a significant reduction in BSMC
617 contraction transfected with sgRNA-*BAIAP2L1* when compared to scramble sgRNA
618 transfected and ACh stimulated (Fig. 7b-c). We saw no significant differences in BSMC
619 contraction between sgRNA-*ERDR1* transfected and scramble sgRNA transfected

620 and ACh stimulated cells (Fig. 7b-c). Taken together, this data indicates that
621 *BAIAP2L1* a gene that was downregulated in IgM-deficient mice has a stimulant-
622 specific role in inducing airway contraction of bronchial smooth muscle cells during
623 asthma.
624
625 **DISCUSSION**
626 Here, we described an unexpected function of IgM in the regulation of
627 bronchoconstriction. We show by RNA sequencing that in the lung tissue of IgM-
628 deficient mice, there is a reduction in genes (*Baiap2l1* and *Erdr1*) associated with actin
629 cytoskeleton and re-arrangement, a key factor in smooth muscle contraction and AHR.
630 We used single-cell force cytometry and CRISPR-Cas9 technology to validate these
631 genes in the human BSM cell line and show as a proof of concept that deletion of
632 *BAIAP2L1* reduced muscle contraction in a stimulant-specific manner.
633
634 B cells play a complex role in allergic asthma, earlier studies using B cell-deficient
635 mice showed a redundant role of B cells in OVA-induced allergic airway inflammation
636 and airway hyperreactivity [27–29]. We and others have recently shown using a more
637 complex allergen HDM relevant to human asthma that antigen load is crucial in B cell
638 function [22–24]. We explored these possibilities in the context of IgM deficiency and
639 observed a profound reduction in AHR. This was in complete contrast to what has
640 been observed in B cell-deficient mice and in IgE or FcεRI-deficient mice [23,24,30]. We
641 also found a similar reduction in AHR at higher doses of HDM, albeit less pronounced.
642 Reduction in AHR was not only specific to HDM, but we also found reduced AHR in
643 IgM-deficient mice sensitised with OVA complexed to alum and challenged with OVA,
644 although less pronounced. AHR reduction in IgM-deficient mice was also seen in the

645 acute papain model which only activates innate responses including innate lymphoid
646 cells [46]. Interestingly, this reduction in AHR was not associated with reduced allergic
647 airway inflammation including eosinophilia, mucus production or Th2 cells in all
648 models tested, which was unexpected considering these features are key in AHR. B
649 cell-deficient mice show a reduction in eosinophilia and antigen-specific Th2 cells at
650 low doses of HDM, which leads to reduced AHR [24]. Similar findings are observed in
651 mice lacking IL-4Rα specifically in B cells when challenged with HDM [22].
652
653 IgM deficiency did not impact B cell development in primary and secondary lymphoid
654 tissues and accumulation of follicular and germinal centre B cells. Interestingly, there
655 was a lack of class switching to IgG1 and IgE isotypes despite increased expression
656 of IgD. The lack of class switching to IgG1 and IgE contrasts with earlier reports, which
657 suggested that IgD can largely replace IgM for class switching to other isotypes,
658 resulting in delayed neutralising IgG1 against vesicular stomatitis virus (VSV) [32,47]. To
659 get a better understanding of which IgM function was responsible for AHR, we showed
660 that the transfer of naïve wild-type mice serum to IgM-deficient mice could restore IgE
661 production and HDM-specific IgE and IgG1. This is consistent with what has been
662 observed in the context of influenza viral infections, where the transfer of purified or
663 serum IgM into B cell-deficient mice restored IgM-induced viral neutralisation [48]. We
664 believe that naïve sera transferred to IgM-deficient mice were able to bind to the
665 surface of B cells via IgM receptors (FcμR / Fcα/μR), which are still present on IgM-
666 deficient B cells, and this signalling is sufficient to facilitate Class Switch
667 Recombination (CSR). This was also confirmed by the ability of B cells to reach
668 germinal centres in IgM-deficient mice during HDM exposure. Our $IgM^{-/-}$ mouse lacks
669 both membrane-bound and secreted IgM, and transferred serum contains at least

670 secreted IgM which can bind to B cell surfaces. Of course, we can't rule out that
671 transferred sera from WT mice also contains some IgG1 which can facilitate class
672 switching to IgE when transferred to IgM-deficient mice. Despite the ability of wild-type
673 serum to restore IgE, it was not enough to restore AHR, which may be due to the
674 difficulties in restoring IgM to normal levels (200-800 μg). Our findings on the
675 redundant role of IgE were consistent with previous studies where IgE nor its high-
676 affinity receptor (FcεRI) were essential in AHR in an HDM or OVA model [30]. The lack
677 of functional role of serum-transferred IgE was consistent with earlier findings on *H.*
678 *polygyrus* transfer of immune serum where IgE was found not to be essential in
679 protection against *H. polygyrus* re-infection [37]. To resolve other endogenous factors
680 that could have potentially influenced reduced AHR in IgM-deficient mice, we resorted
681 to busulfan chemical irradiation to deplete bone marrow cells in IgM-deficient mice and
682 replace bone marrow with WT bone marrow. While it is well accepted that busulfan
683 chemical irradiation partially depletes bone marrow cells, in our case it was not
684 possible to pursue other irradiation methods due to changes in ethical regulations and
685 that fact that mice are slow to recover after gamma rays irradiation. Busulfan chemical
686 irradiation allowed us to show that we could mostly restore AHR in IgM-deficient
687 recipient mice that received donor WT bone marrow when challenged with low dose
688 HDM.
689
690 B cell isotype IgD has been shown to promote Th2 cells and OVA-, papain- and NP-
691 specific humoral responses specifically IgG1 and IgE through basophil activation [31].
692 IgD has also been shown to inhibit IgE-mediated basophil activation through
693 downregulation of genes associated with cytoskeleton organisation such as signal
694 transducers phosphoinositide-3 kinase, RAS, and RHO [31]. Our RNA sequencing data

695 showed downregulation of *Baiap2l1* and *Erdr1* in IgM-deficient mice, genes which
696 have been shown to associate with actin cytoskeleton and re-arrangement, [41,42,49].
697 Contraction of the ASM is central to AHR as it controls airway diameter and airflow
698 which can increase resistance [50]. ASM activated by cytokines such as IL-13 or TNF-α
699 or bronchoconstrictor ACh induces cytosolic calcium accumulation [50,51]. Ca^{2+} release
700 results in a cascade of events that involves kinases and phosphorylation of key
701 molecules such as actin and myosin involved in smooth muscle contraction [45]. Gene
702 set enrichment analysis suggested that genes downregulated in IgM-deficient mice
703 were involved in processes such as muscle contraction, muscle twitching, skeletal
704 muscle movement. As a proof of concept we validated the involvement of *BAIAP2L1*
705 in bronchial smooth muscle contraction using a high throughput method that allows us
706 to measure contraction of 1000s of single cells [44]. When we deleted *BAIAP2L1* using
707 CRISPR-Cas9, we showed that deletion of *BAIAP2L1* in BSMCs reduced smooth
708 muscle contraction when stimulated with TNF-α and ACh, but not IL-13. Deletion of
709 ERDR1 had minor impact on muscle contraction across different stimulants
710 suggesting a stimulant and gene-specific role. IRTKS/BAIAP2L1 has been shown to
711 regulate microvilli elongation by forming a complex with actin-regulating protein EPS8
712 [41]. In this setting IRTKS elongate microvilli via distinct mechanisms that require
713 functional WH2 and SH3 domains, which binds EPS8, an F-actin capping and bundling
714 protein [41]. We have not fully dissected how *BAIAP2L1* could be regulated by IgM, but
715 it is clear that through its actions to regulate actin bundling, it is involved in muscle
716 contraction which requires actin and myosin head interaction (summarised in Fig. 8).
717
718 We speculate that IgM can directly activate smooth muscle cells by binding a number
719 of its surface receptors including FcμR, Fcα/μR and pIgR [52–54]. IgM binds to FcμR

720 strictly, but shares Fcα/μR and pIgR with IgA [5,52,54]. Both Fcα/μR and pIgR can be
721 expressed by non-structural cells at mucosal sites [54,55]. We would not rule out that the
722 mechanisms of muscle contraction might be through one of these IgM receptors,
723 especially the ones expressed on smooth muscle cells[54,55]. Certainly, our future
724 studies will be directed towards characterizing the mechanism by which IgM potentially
725 activates the smooth muscle.
726
727 We believe these findings report for the first time an independent function of IgM from
728 its natural class switching and non-specific binding to microbial components. We
729 believe that IgM function in regulating ASM may be indirect through other unknown
730 factors but does not involve microbiota as treatment of mice with a mixture of
731 antibiotics did not restore AHR. Early vaccination with bacterial species, such as group
732 *A streptococcus* containing GlcNAc or β-1,3-glucans can protect adult mice against *A.*
733 *fumigatus*-induced allergic asthma [56]. This is mainly through conserved germline-
734 encoded IgM antibodies, which have broad specificities to common allergens
735 containing GlcNAc moieties such as Dermatophytes [8,57]. Together these findings
736 demonstrate for the first time an important function of IgM in regulating airway
737 hyperresponsiveness independent of the presence of T helper 2 allergic inflammation.
738 These findings have implications for future treatment of allergic asthma through
739 bronchodilators.
740
741 **Competing interests**
742 The authors declare that they have no competing interests.
743
744

745 **Acknowledgements**

746 We thank the UCT Research Animal Facility for maintaining mice, and Munadia Ansari
747 for genotyping mice. We are grateful to Lizette Fick, Matt Darby and Raygaana Jacobs
748 for their excellent histology services and the UCT Confocal Microscopy Core Facilities.
749 We are grateful to Ronnie Dreyer for the excellent cell sorting and Flow Cytometry
750 Core Facility. We thank FlowJo for proving free service to Africa.

751

752 **Author contributions**

753 Conceived and supervised study: SH FB. Performed the experiments: SH AFS JK KJ
754 NM MS AN FM HN WM. Analysed the data: SH AFS KJ JO NM HN FM. Wrote the
755 paper: SH FB. All authors discussed the results and commented on the manuscript.

756

757 **Funding statement**

758 This work was supported by ICGEB, Cape Town Component, Medical Research
759 Council (MRC) South Africa as well as support by the South African National Research
760 Foundation (NRF) Research Chair initiative (SARChi) and Wellcome Trust CIDRI-
761 Africa (203135Z/16/Z) to FB. SH is supported by NRF Thuthuka Grant (117721), NRF
762 Competitive Support for Unrated Researcher (138072), MRC South Africa under Self-
763 initiated grant. NM was supported by the South African MRC PhD Fellowship and
764 ATAP Fellowship at UCT. AN was supported by NRF MSc Scholarship. This research
765 was funded in whole, or in part, by the Wellcome Trust [Grant number 203135Z/16/Z].
766 For the purpose of open access, the author has applied a CC BY public copyright
767 licence to any Author Accepted Manuscript version arising from this submission.

768

769 **References**

770 1. Akula, S., Mohammadamin, S. & Hellman, L. Fc Receptors for Immunoglobulins and
771 Their Appearance during Vertebrate Evolution. *PLoS One* **9**, e96903 (2014).
772 2. Blandino, R. & Baumgarth, N. Secreted IgM: New tricks for an old molecule. *J Leukoc*
773 *Biol* **106**, 1021–1034 (2019).
774 3. Baumgarth, N. *et al.* B-1 and B-2 Cell–Derived Immunoglobulin M Antibodies Are
775 Nonredundant Components of the Protective Response to Influenza Virus Infection.
776 *Journal of Experimental Medicine* **192**, 271–280 (2000).
777 4. Ehrenstein, M. R. & Notley, C. A. The importance of natural IgM: scavenger, protector
778 and regulator. *Nat Rev Immunol* **10**, 778–786 (2010).
779 5. Michaud, E., Mastrandrea, C., Rochereau, N. & Paul, S. Human Secretory IgM: An
780 Elusive Player in Mucosal Immunity. *Trends Immunol* **41**, 141–156 (2020).
781 6. Quartier, P., Potter, P. K., Ehrenstein, M. R., Walport, M. J. & Botto, M. Predominant
782 role of IgM-dependent activation of the classical pathway in the clearance of dying
783 cells by murine bone marrow-derived macrophages in vitro. *Eur J Immunol* **35**, 252–
784 260 (2005).
785 7. Wesemann, D. R. *et al.* Microbial colonization influences early B-lineage development
786 in the gut lamina propria. *Nature* **501**, 112–115 (2013).
787 8. New, J. S. *et al.* Neonatal Exposure to Commensal-Bacteria-Derived Antigens Directs
788 Polysaccharide-Specific B-1 B Cell Repertoire Development. *Immunity* **53**, 172-186.e6
789 (2020).
790 9. Kawahara, T., Ohdan, H., Zhao, G., Yang, Y.-G. & Sykes, M. Peritoneal Cavity B Cells
791 Are Precursors of Splenic IgM Natural Antibody-Producing Cells. *The Journal of*
792 *Immunology* **171**, 5406 LP – 5414 (2003).
793 10. Nguyen, T. T. T., Graf, B. A., Randall, T. D. & Baumgarth, N. sIgM–FcμR Interactions
794 Regulate Early B Cell Activation and Plasma Cell Development after Influenza Virus
795 Infection. *The Journal of Immunology* **199**, 1635 LP – 1646 (2017).
796 11. Jones, K., Savulescu, A. F., Brombacher, F. & Hadebe, S. Immunoglobulin M in Health
797 and Diseases: How Far Have We Come and What Next? . *Frontiers in*
798 *Immunology* vol. 11 2858 Preprint at
799 https://www.frontiersin.org/article/10.3389/fimmu.2020.595535 (2020).
800 12. Yilmaz, B. *et al.* Gut Microbiota Elicits a Protective Immune Response against Malaria
801 Transmission. *Cell* **159**, 1277–1289 (2014).
802 13. Krishnamurty, A. T. *et al.* Somatically Hypermutated Plasmodium-Specific IgM+
803 Memory B Cells Are Rapid, Plastic, Early Responders upon Malaria Rechallenge.
804 *Immunity* **45**, 402–414 (2016).
805 14. Rapaka, R. R. *et al.* Conserved natural IgM antibodies mediate innate and adaptive
806 immunity against the opportunistic fungus Pneumocystis murina. *Journal of*
807 *Experimental Medicine* **207**, 2907–2919 (2010).
808 15. Subramaniam, K. S. *et al.* The absence of serum IgM enhances the susceptibility of
809 mice to pulmonary challenge with Cryptococcus neoformans. *J Immunol* **184**, 5755–
810 5767 (2010).
811 16. Magri, G. *et al.* Human Secretory IgM Emerges from Plasma Cells Clonally Related to
812 Gut Memory B Cells and Targets Highly Diverse Commensals. *Immunity* **47**, 118-
813 134.e8 (2017).

814 17. Weber, G. F. *et al.* Pleural innate response activator B cells protect against
815 pneumonia via a GM-CSF-IgM axis. *Journal of Experimental Medicine* **211**, 1243–1256
816 (2014).
817 18. del Barrio, L. *et al.* Production of Anti-LPS IgM by B1a B Cells Depends on IL-1β and Is
818 Protective against Lung Infection with Francisella tularensis LVS. *PLoS Pathog* **11**,
819 e1004706 (2015).
820 19. Goldstein, M. F. *et al.* Selective IgM immunodeficiency: retrospective analysis of 36
821 adult patients with review of the literature. *Annals of Allergy, Asthma & Immunology*
822 **97**, 717–730 (2006).
823 20. Lambrecht, B. N. & Hammad, H. The immunology of asthma. *Nat Immunol* **16**, 45–56
824 (2014).
825 21. Mandler, R., Finkelman, F. D., Levine, A. D. & Snapper, C. M. IL-4 induction of IgE class
826 switching by lipopolysaccharide-activated murine B cells occurs predominantly
827 through sequential switching. *The Journal of Immunology* **150**, 407 LP – 418 (1993).
828 22. Hadebe, S. *et al.* Deletion of IL-4Ra signaling on B cells limits hyperresponsiveness
829 depending on antigen load. *Journal of Allergy and Clinical Immunology* **148**, 99-109.e5
830 (2021).
831 23. Habener, A. *et al.* Regulatory B cells control airway hyperreactivity and lung
832 remodeling in a murine asthma model. *Journal of Allergy and Clinical Immunology*
833 **147**, 2281-2294.e7 (2021).
834 24. Dullaers, M. *et al.* House dust mite–driven asthma and allergen-specific T cells
835 depend on B cells when the amount of inhaled allergen is limiting. *Journal of Allergy*
836 *and Clinical Immunology* **140**, 76-88.e7 (2017).
837 25. Ballesteros-Tato, A. *et al.* T Follicular Helper Cell Plasticity Shapes Pathogenic T Helper
838 2 Cell-Mediated Immunity to Inhaled House Dust Mite. *Immunity* **44**, 259–273 (2016).
839 26. Wypych, T. P., Marzi, R., Wu, G. F. & Lanzavecchia, A. Role of B cells in T H cell
840 responses in a mouse model of asthma. *Journal of Allergy and Clinical Immunology*
841 **141**, 1395–1410 (2020).
842 27. MacLean, J. A., Sauty, A., Luster, A. D., Drazen, J. M. & De Sanctis, G. T. Antigen-
843 induced airway hyperresponsiveness, pulmonary eosinophilia, and chemokine
844 expression in B cell-deficient mice. *Am J Respir Cell Mol Biol* **20**, 379–387 (1999).
845 28. Hamelmann, E. *et al.* Development of Eosinophilic Airway Inflammation and
846 Airway Hyperresponsiveness Requires Interleukin-5 but Not Immunoglobulin E or B
847 Lymphocytes. *Am J Respir Cell Mol Biol* **21**, 480–489 (1999).
848 29. Korsgren, M., ält, J. S. E., Korsgren, O., Sundler, F. & Persson, C. G. A. Allergic
849 Eosinophil-rich Inflammation Develops in Lungs and Airways of B Cell–deficient Mice.
850 *Journal of Experimental Medicine* **185**, 885–892 (1997).
851 30. McKnight, C. G., Jude, J. A., Zhu, Z., Panettieri, R. A. & Finkelman, F. D. House Dust
852 Mite–Induced Allergic Airway Disease Is Independent of IgE and FcεRIα. *Am J Respir*
853 *Cell Mol Biol* **57**, 674–682 (2017).
854 31. Shan, M. *et al.* Secreted IgD Amplifies Humoral T Helper 2 Cell Responses by Binding
855 Basophils via Galectin-9 and CD44. *Immunity* **49**, 709-724.e8 (2018).
856 32. Lutz, C. *et al.* IgD can largely substitute for loss of IgM function in B cells. *Nature* **393**,
857 797–801 (1998).
858 33. Montecino-Rodriguez, E. & Dorshkind, K. Use of Busulfan to Condition Mice for Bone
859 Marrow Transplantation. *STAR Protoc* **1**, 100159 (2020).

860 34. Kirstein, F., Nieuwenhuizen, N. E., Jayakumar, J., Horsnell, W. G. C. & Brombacher, F.
861 Role of IL-4 receptor α–positive CD4+ T cells in chronic airway hyperresponsiveness.
862 *Journal of Allergy and Clinical Immunology* (2015) doi:10.1016/j.jaci.2015.10.036.
863 35. Wu, T. *et al.* clusterProfiler 4.0: A universal enrichment tool for interpreting omics
864 data. *The Innovation* **2**, (2021).
865 36. Muramatsu, M. *et al.* Class Switch Recombination and Hypermutation Require
866 Activation-Induced Cytidine Deaminase (AID), a Potential RNA Editing Enzyme. *Cell*
867 **102**, 553–563 (2000).
868 37. Wojciechowski, W. *et al.* Cytokine-Producing Effector B Cells Regulate Type 2
869 Immunity to H. polygyrus. *Immunity* **30**, 421–433 (2009).
870 38. Smith, F. L. *et al.* B-1 plasma cells require non-cognate CD4 T cell help to generate a
871 unique repertoire of natural IgM. *Journal of Experimental Medicine* **220**, e20220195
872 (2023).
873 39. Trompette, A. *et al.* Gut microbiota metabolism of dietary fiber influences allergic
874 airway disease and hematopoiesis. *Nat Med* **20**, 159–166 (2014).
875 40. Norderhaug, I. N., Johansen, F.-E., Krajči, P. & Brandtzaeg, P. Domain deletions in the
876 human polymeric Ig receptor disclose differences between its dimeric IgA and
877 pentameric IgM interaction. *Eur J Immunol* **29**, 3401–3409 (1999).
878 41. Postema, M. M., Grega-Larson, N. E., Neininger, A. C. & Tyska, M. J. IRTKS (BAIAP2L1)
879 Elongates Epithelial Microvilli Using EPS8-Dependent and Independent Mechanisms.
880 *Current Biology* **28**, 2876-2888.e4 (2018).
881 42. Abo, H. *et al.* Erythroid differentiation regulator-1 induced by microbiota in early life
882 drives intestinal stem cell proliferation and regeneration. *Nat Commun* **11**, 1–12
883 (2020).
884 43. James, A. L. *et al.* Airway Smooth Muscle Hypertrophy and Hyperplasia in Asthma. *Am*
885 *J Respir Crit Care Med* **185**, 1058–1064 (2012).
886 44. Pushkarsky, I. *et al.* Elastomeric sensor surfaces for high-Throughput single-cell force
887 cytometry. *Nat Biomed Eng* **2**, 124–137 (2018).
888 45. Ouedraogo, N. & Roux, E. Pulmonary & Respiratory Medicine Physiology of Airway
889 Smooth Muscle Contraction : An Overview. *J Pulm Respir Med* **4**, 1–6 (2014).
890 46. Darby, M. *et al.* ILC3-derived acetylcholine promotes protease-driven allergic lung
891 pathology. *Journal of Allergy and Clinical Immunology* **147**, 1513-1516.e4 (2021).
892 47. Ochsenbein, A. F. *et al.* Control of Early Viral and Bacterial Distribution and Disease by
893 Natural Antibodies. *Science (1979)* **286**, 2156 LP – 2159 (1999).
894 48. Jayasekera, J. P., Moseman, E. A. & Carroll, M. C. Natural Antibody and Complement
895 Mediate Neutralization of Influenza Virus in the Absence of Prior Immunity. *J Virol* **81**,
896 3487 LP – 3494 (2007).
897 49. Houh, Y. K., Kim, K. E., Park, H. J. & Cho, D. Roles of erythroid differentiation regulator
898 1 (Erdr1) on inflammatory skin diseases. *Int J Mol Sci* **17**, 1–10 (2016).
899 50. Perkins, C. *et al.* Selective stimulation of IL-4 receptor on smooth muscle induces
900 airway hyperresponsiveness in mice. *J Exp Med* **208**, 853–867 (2011).
901 51. Moulton, B. C. & Fryer, A. D. Muscarinic receptor antagonists, from folklore to
902 pharmacology; finding drugs that actually work in asthma and COPD. *Br J Pharmacol*
903 **163**, 44–52 (2011).
904 52. Nguyen, T. T. T. *et al.* The IgM receptor FcμR limits tonic BCR signaling by regulating
905 expression of the IgM BCR. *Nat Immunol* **18**, 321–333 (2017).

53. Shibuya, A. *et al.* Fcα/μ receptor mediates endocytosis of IgM-coated microbes. *Nat Immunol* **1**, 441–446 (2000).
54. Liu, J. *et al.* Role of the IgM Fc Receptor in Immunity and Tolerance. *Front Immunol* **10**, (2019).
55. Kim, M.-S. *et al.* A draft map of the human proteome. *Nature* **509**, 575–581 (2014).
56. Kin, N. W., Stefanov, E. K., Dizon, B. L. P. & Kearney, J. F. Antibodies Generated against Conserved Antigens Expressed by Bacteria and Allergen-Bearing Fungi Suppress Airway Disease. *The Journal of Immunology* **189**, 2246 LP – 2256 (2012).
57. Kearney, J. F., Patel, P., Stefanov, E. K. & King, R. G. Natural Antibody Repertoires: Development and Functional Role in Inhibiting Allergic Airway Disease. *Annu Rev Immunol* **33**, 475–504 (2015).

919 **FIGURE LEGENDS**

920

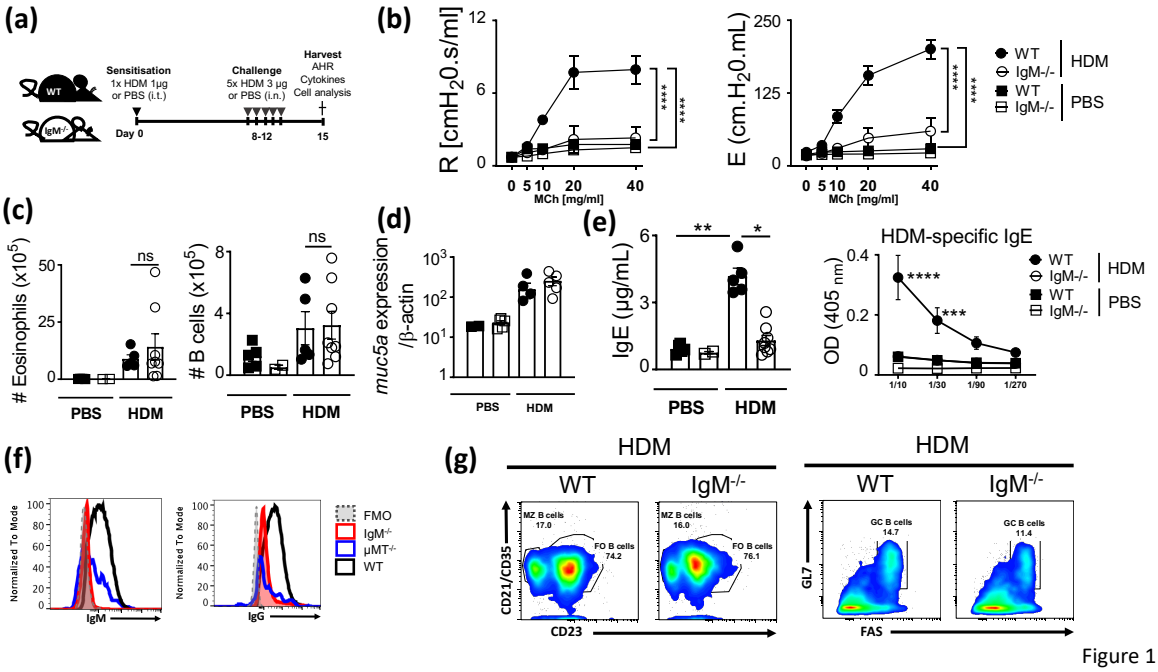

Figure 1

921

922 **Fig. 1 IgM-deficiency leads to reduced airway hyperresponsiveness and class**

923 **switching to IgE in HDM-induced asthma.**

924 **a** Schematic diagram showing sensitisation and challenge protocol where mice (IgM^{-}

925 $^{/-}$) and wild type littermate control (WT) were sensitised with HDM 1 µg intra-tracheally

926 on days 0 and challenged with HDM 3 µg on days 8-12. Analysis was done on day 15.

927 **b** Airway resistance and elastance were measured with increasing doses of acetyl

928 methacholine (0 -40 mg/mL).

929 **c** Total lung eosinophil numbers (live^{+}Siglec-F^{+}CD11c^{-}) and B cells

930 (live^{+}B220^{+}CD19^{+}MHCII^{+}) were stained and analysed by Flow cytometry and

931 enumerated from % of live cells.

932 **d** *Muc5a* gene expression in whole lung tissue.

933 **e** Total IgE and HDM-specific IgE in serum.

934 **f** IgG1 and IgM surface expression in mediastinal lymph node B cells of WT, $IgM^{-/-}$ and
935 $\mu MT^{-/-}$ mice.

936 **g** Marginal Zone ($live^{+}B220^{+}CD19^{+}MHCII^{+}CD21/CD35^{+}CD23^{-}$), follicular
937 ($live^{+}B220^{+}CD19^{+}MHCII^{+}CD23^{+}CD21/CD35^{+}$) and Germinal Centre
938 ($live^{+}B220^{+}CD19^{+}MHCII^{+}GL7^{+}FAS^{+}$) B cells in the mediastinal lymph node of WT and
939 $IgM^{-/-}$ mice challenged with HDM.

940 Shown is mean ± SEM from two pooled experiments (n=7 - 10). Significant differences
941 between groups were performed by Student *t*-test (Mann-Whitney) (c, d, e) or by Two-
942 Way ANOVA with Benforroni post-test (b) and are described as: *$p<0.05$, **$p<0.01$,
943 ***$p<0.001$, ****$p<0.0001$.

944

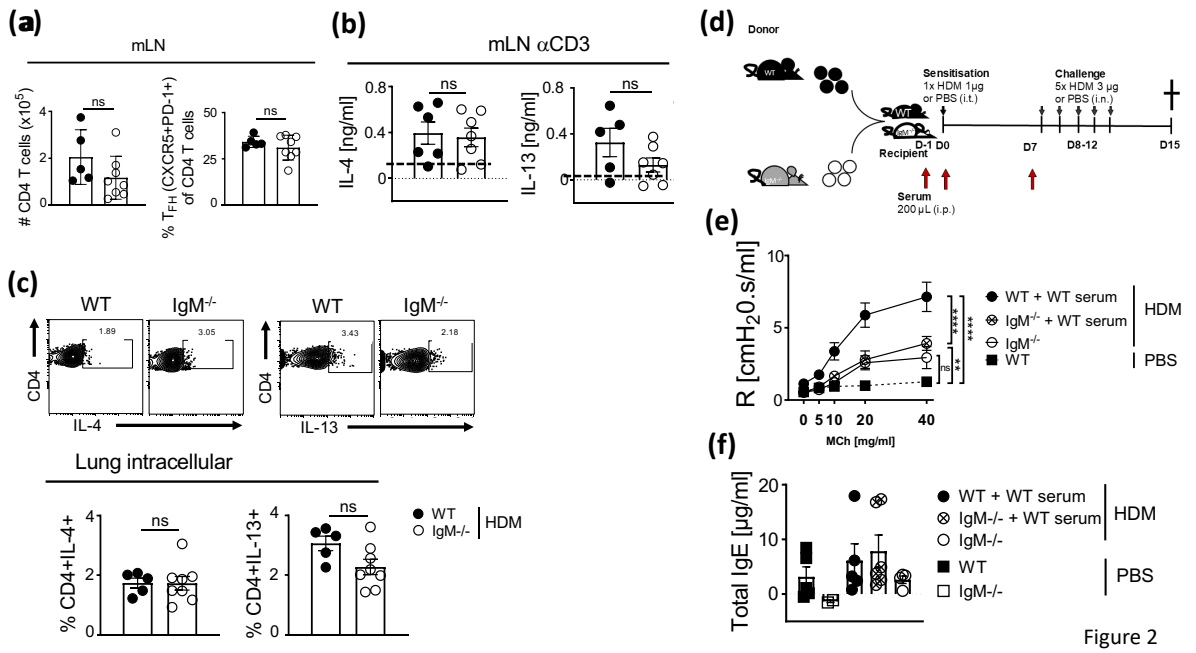

Fig. 2 IgM-deficiency does not lead to reduced Th2 allergic airway inflammation and serum transfer restores IgE, but not AHR. Fig. a-c, mice treated as in Fig. 1a.

a Total mediastinal lymph node CD4 T cell numbers (live$^+$CD3$^+$CD4$^+$) and % of Follicular Helper T cells (live$^+$CD3$^+$CD4$^+$PD-1$^+$CXCR5$^+$) of CD4 T cells were stained and analysed by Flow cytometry and enumerated from % of live cells.

b Mediastinal lymph nodes were stimulated with anti-CD3 (10µg/mL) for 5 days and supernatants were used to measure levels of IL-4 and IL-13. Cytokines were not detected in unstimulated or HDM (30µg) stimulated mLN.

c Representative FACS plots and frequencies of lung CD4 T cells (live$^+$CD3$^+$CD4$^+$) producing IL-4 and IL-13 after 5 hr stimulation with PMA/ionomycin in the presence of monensin.

d Schematic diagram showing serum transfer from WT to IgM$^{-/-}$ which were then sensitised as shown in Fig 1,a.

959 **e** Airway resistance was measured with increasing doses of acetyl methacholine (0 -
960 40 mg/mL).

961 **f** Total IgE in serum of mice either transferred with WT serum, $IgM^{-/-}$ serum or no
962 serum.

963 Shown is the mean ± SEM from two pooled experiments (n=5 - 8). Significant
964 differences between groups were performed by Student *t*-test (Mann-Whitney) (C, D,
965 E) or by Two-*Way ANOVA with Benforroni post-test (B) and are described as: *p<0.05,*
966 **p<0.01, ****p*<0.001, *****p*< 0.0001.

967

968

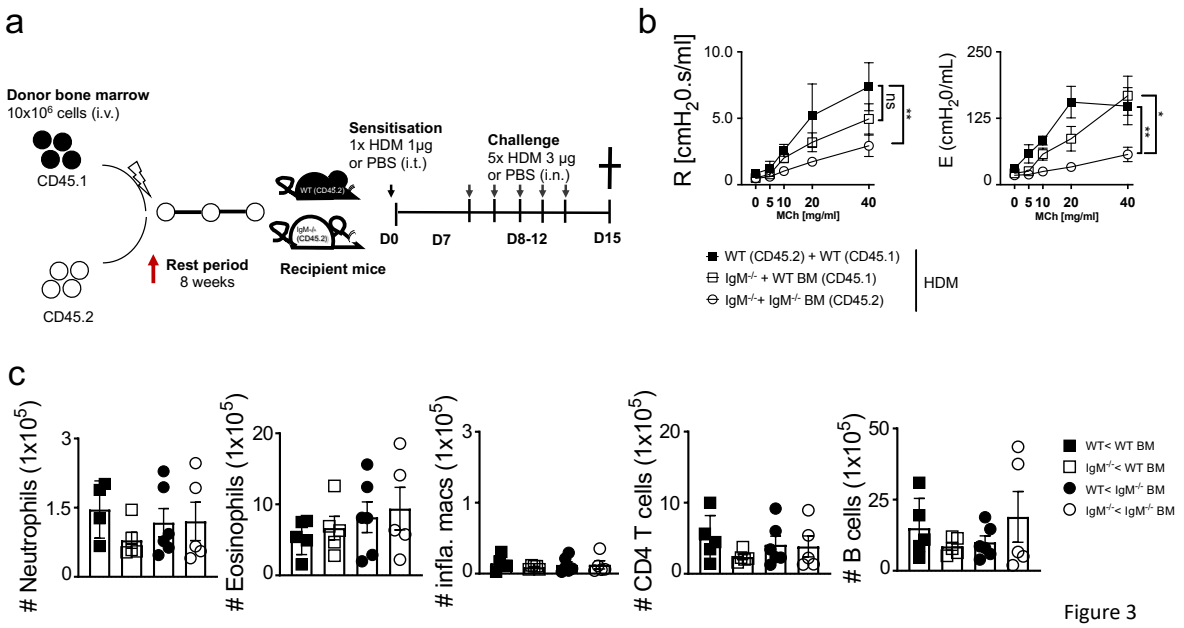

Fig. 3 Partial wild type bone marrow replenishment restores AHR in IgM-deficient mice (Fig. a-c, mice treated as in Fig. 1a).

a Schematic diagram showing WT and IgM-deficient mice being chemically irradiated with busulfan (25 mg per day for 3 days) and adoptively transferred with congenic bone marrow ($10x10^6$ per mouse intravenously) at day 4. Mice (WT to $IgM^{-/-}$ plus bone marrow) were then rested for 8 weeks before being sensitised as shown in Fig 1,a.

b Airway resistance and elastance were measured with increasing doses of acetyl methacholine (0 -40 mg/mL).

c Total lung neutrophils ($live^+CD11b^+Ly6G^+$), eosinophils ($live^+Siglec\text{-}F^+CD11c^-$), inflammatory macrophages ($live^+Ly6G^-CD11b^+F4/80^+$), CD4 T cells ($live^+CD3^+CD4^+CD8^-$) and B cells ($live^+B220^+CD19^+MHCII^+$) were stained and analysed by Flow cytometry and enumerated from % of live cells.

Shown is the mean ± SD from one experiments (n=5 – 6 per group). Significant differences between groups were performed by Student *t*-test (Mann-Whitney) (C) or

984 by Tw*o-Way ANOVA* with Benforroni post-test (B) and are described as: *p<0.05,

985 **p<0.01, ***p<0.001, ****p< 0.0001.

986

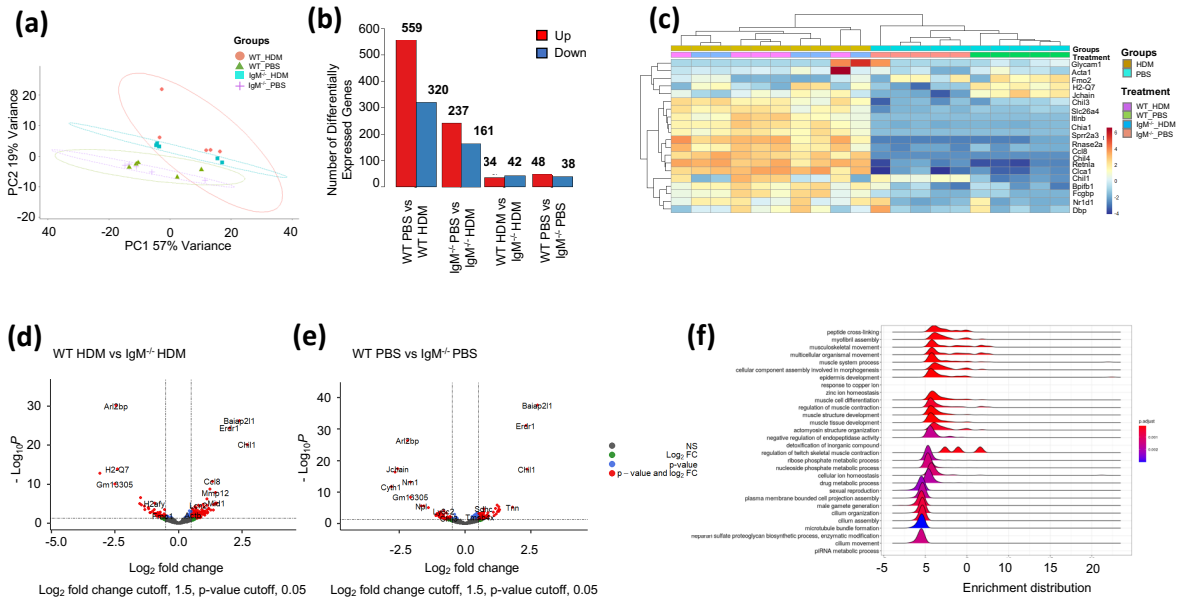

Figure 4

Fig. 4 Genes associated with muscle contraction are downregulated in IgM-deficient mice. WT and IgM$^{-/-}$ mice were treated as in Figure 1A and RNA was collected from the whole lung for RNA sequencing.

a Principal-component (PC) analysis showing variation in the global gene expression profiles across the different groups. PC1 (60%) and PC2 (18%), which capture the greatest variation in gene expression, are shown. Orange colour represents WT HDM, green colour represents WT PBS, Blue colour represents IgM$^{-/-}$ HDM and purple crosses represent IgM$^{-/-}$ PBS. Each dot represents an individual mouse.

b Number of differentially expressed genes between groups.

c Heatmaps depicting the differently expressed genes between WT and IgM$^{-/-}$ samples from HDM-treated and PBS mice ranked based on hierarchical clustering.

d-e Volcano plots: numbers and colour relate to genes that have an adjusted *p* value <0.05. Blue, significantly downregulated; red, significantly up regulated; grey, non-differentially expressed. P values were adjusted for multiple testing using the

1004 Benjamini-Hochberg method. (D) represent changes between WT and IgM$^{-/-}$ treated
1005 with HDM and (E) represents changes between WT and IgM$^{-/-}$ treated with saline.
1006 **f** Gene set enrichment analysis (GSEA) of hallmark gene sets from the Molecular
1007 Signatures Database of the Broad Institute, showing the normalized enrichment
1008 scores (NES) for lung RNA-Seq data from WT mice.
1009
1010

1011

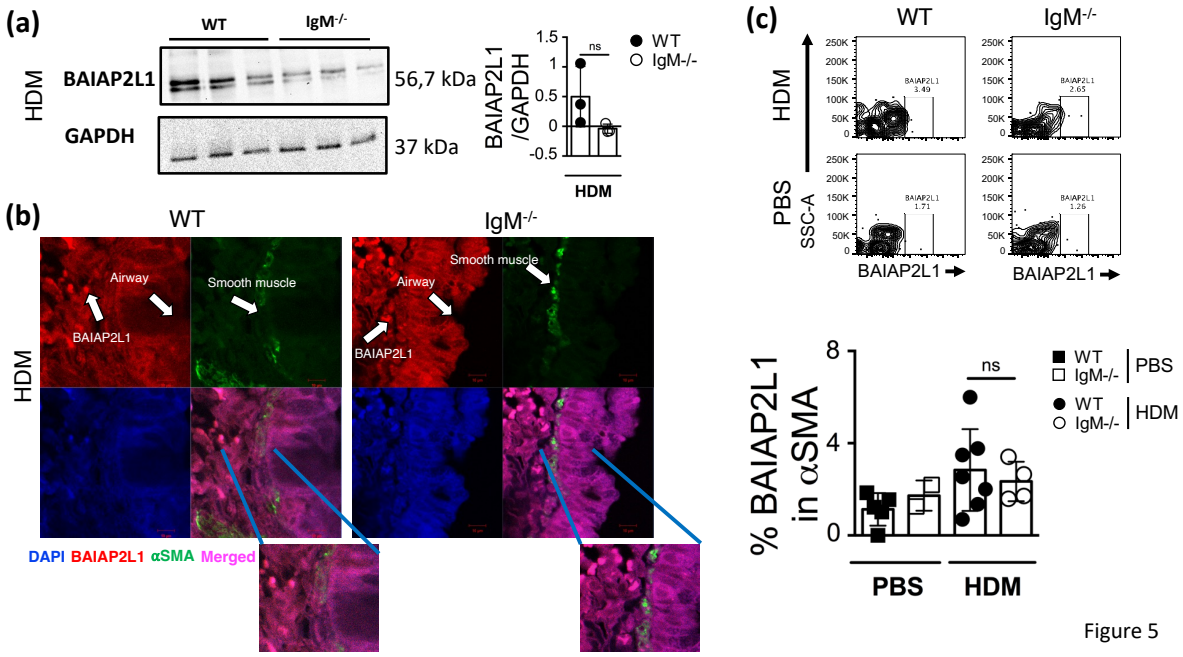

Figure 5

1012

1013 **Fig. 5 *BAIAP2L1* is expressed in close contact to smooth muscle.**

1014 **a** Mouse lungs were homogenised in RIPA buffer and blotted on nitrocellulose.

1015 Rabbit anti-human BAIAP2L1 and mouse anti-GAPDH was used as primary

1016 antibody. Lines 1-3 is WT mice, lines 4-6 is IgM$^{-/-}$ mice sensitised and challenged

1017 with HDM.

1018 **b** Lung sections from WT and IgM$^{-/-}$ mice sensitised and challenged with HDM were

1019 immunostained for nuclei stained DAPI (Blue), anti-BAIAP2L1 (red), α smooth

1020 muscle actin (green) and merged images (Magenta). Insert below shows zoomed in

1021 image of merged BAIAP2L1 and α smooth muscle actin.

1022 **c** Representative flow cytometry plots showing BAIAP2L1 expression

1023 (Live^{+}Singlets^{+}CD45^{-}α SMA^{+}BAIAP2L1^{+}) in WT and IgM$^{-/-}$ treated with HDM or PBS.

1024 Quantification of % BAIAP2L1 in α smooth muscle actin is shown.

1025

1026 Shown are representative images from 2 independent experiments (n= 3 mice per

1027 group).

1028

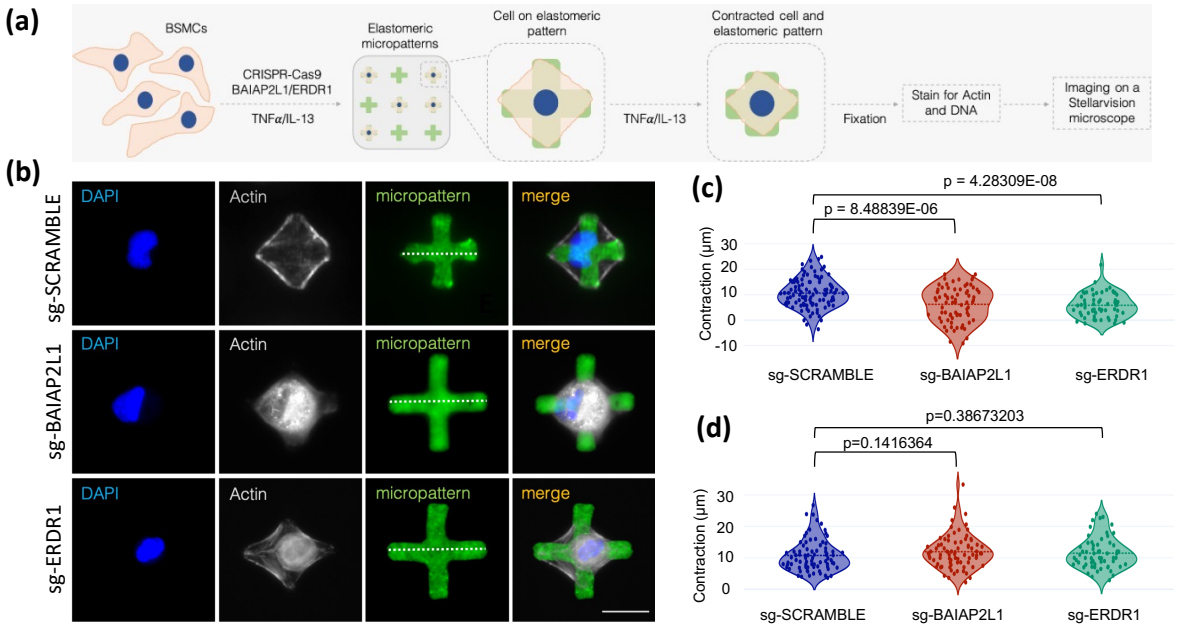

Figure 6

Fig. 6 CRISPR-based deletion of *BAIAP2L1* leads to reduced smooth muscle contraction at a single-cell level.

a, Bronchial smooth muscle cells (1.6×10^5 cells/well) were transfected with CRISPR-Cas9 single guide RNAs (scramble, *BAIAP2L1* and *ERDR1*), stimulated with recombinant human IL-13 (100 ng/mL) and TNF-α (10 ng/mL) for 48 h. Cells were then transferred to elastomeric micropatterns, stimulated again with rIL-13 and rTNF-α and fixed before imaging on a StellarVision microscope. **b**, Representative images of single BSMCs on micropatterns from scramble, *BAIAP2L1* and *ERDR1* stimulated with 10 ng/mL TNF-α. DNA was stained with DAPI, actin fibers with Phaloidin-565 and elastomeric micropatterns are coated in Fibronectin-488. Merged images are shown on the right. **c**, Violin plots showing contraction of 50-100 cells/condition stimulated with 10 ng/mL TNF-α, individual dots represent a single cell contraction, where blue is scramble sgRNA, red is *BAIAP2L1* sgRNA and green is *ERDR1* is sgRNA.

1045 **d**, Violin plots showing contraction of 50-100 cells/condition stimulated with 100 ng/mL
1046 IL-13, individual dots represent a single cell contraction, where blue is scramble
1047 sgRNA, red is *BAIAP2L1* sgRNA and green is *ERDR1* is sgRNA.
1048
1049 Shown is mean ±SEMs from two pooled experiment (n=50 - 100). Significant
1050 differences between groups were performed by student t-test (Mann-Whitney) and *p*
1051 value is shown.
1052

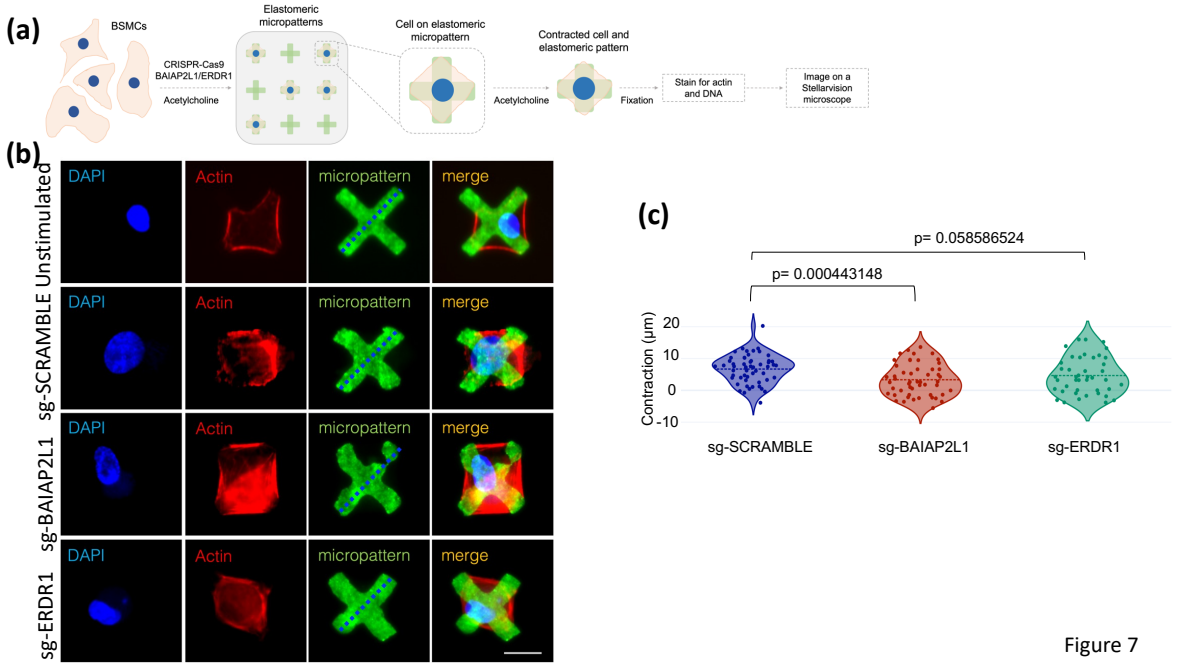

Figure 7

Fig. 7 CRISPR-based deletion of *BAIAP2L1* reduces smooth muscle contraction upon stimulation with acetylcholine.

a Bronchial smooth muscle cells ($1.6x10^5$ cells/well) were transfected with CRISPR-Cas9 single guide RNAs (scramble, *BAIAP2L1* and *ERDR1*), stimulated with Acetylcholine (10µM) for 48 h. Cells were then transferred to elastomeric micropatterns, stimulated again with ACh (10µM) and fixed before imaging on a StellarVision microscope.

b, Representative images of single BSMCs on a single micropattern from unstimulated, scramble, *BAIAP2L1* and *ERDR1* stimulated with ACh (10µM). Shown are DAPI, actin (red), a green fluorescent micropattern and merged images.

c, Violin plots showing contraction of 50-100 cells/condition stimulated with ACh (10µM) individual dots represent a single cell contraction, where blue is scramble sgRNA, red is BAIAP2L1 sgRNA and green is ERDR1 is sgRNA.

1069 Shown is mean ±SD from 1 representative experiment of 2 independent experiments

1070 (n=50 - 100). Significant differences between groups were performed by student t-test

1071 (Mann-Whitney) and *p* value is shown.

1072

1073

1074

1075

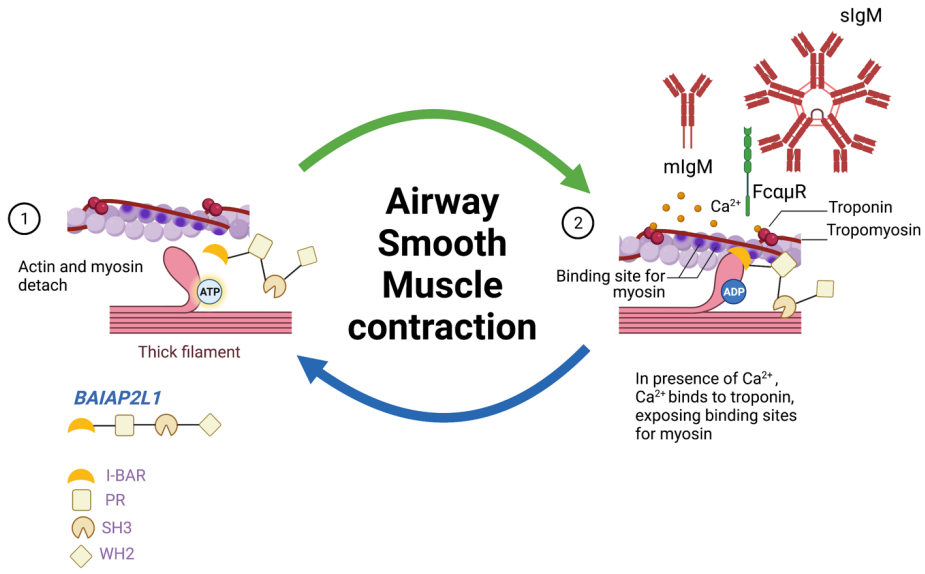

Figure 8

1076

1077 **Fig. 8 Working model showing how *Baiap2l1* could influence muscle contraction**

1078 **through influencing myosin and actin filament interaction. Image adapted from**

1079 **Biorender.**

1080